THE JOURNAL OF PHYSICAL CHEMISTRY Letters

Letter

Cite This: J. Phys. Chem. Lett. 2020, 11, 161−165

pubs.acs.org/JPCL

Real-Time Observation of Fermi Resonances in the S_1 State of Phenol

Kyung Chul Woo† and Sang Kyu Kim*

Department of Chemistry, KAIST, Daejeon 34141, Republic of Korea

Supporting Information

ABSTRACT: Fermi resonances in the first electronically excited (S_1) state of phenol have been observed in real time. Quantum beats associated with coherent superposition of Fermi resonant eigenstates are manifested as temporal oscillations of the ionization cross sections of which the amplitudes are strongly dependent on the total ionization energy. This indicates that coherently excited eigenstates are effectively decomposed into their zeroth-order states, providing the unique opportunity for the investigation of nonstationary state dynamics in real-time. Energy gaps ($\Delta\tilde{\nu}$) of eigenstates within the laser coherence width have been most precisely determined up to date, giving $\Delta\tilde{\nu} \sim 3.302 \pm 0.001$ or 1.655 ± 0.001 cm^{-1} for the $1^1/4^1 10b^1$ or $12^2/8a^1$ Fermi doublets, respectively. Dephasing rate suddenly increases as the S_1 internal energy becomes above ~1500 cm^{-1}, revealing the important role of energy randomization dynamics during the H atom tunneling process of phenol in S_1.

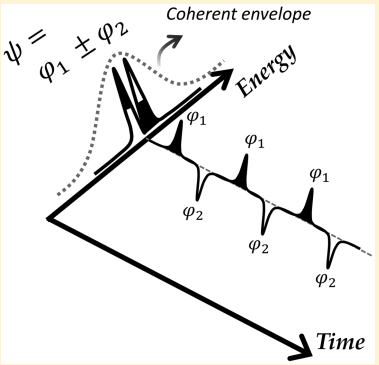

Fermi resonances are misleadingly considered to be quite common in polyatomic molecular systems as there are supposedly many chances for a couple of quantum states belonging to the same irreducible symmetry species to coincide in their vibrational energies. In the ground-state infrared[1−3] or Raman[4−7] spectroscopy, it is often that overtone or combination modes otherwise optically dark obtain significant oscillator strengths because of strong couplings with nearly isoenergetic fundamental modes. Although it is somewhat straightforward to identify Fermi doublets in small molecular systems, it is nontrivial to identify those doublets in vibrational spectra of relatively large polyatomic molecules with many vibrational degrees of freedom.[8−12] Real-time probing of such resonances provides more direct evidence where eigenstates comprising the superposition state are coherently excited within the coherence width of the pump laser pulse. Then quantum interferences of two or more distinct time-dependent wave functions embedded in the superposition state are manifested as oscillatory time-evolution features in various spectroscopic probing schemes. These include laser-induced dispersed fluorescence,[13,14] time-resolved photoion,[15] or photoelectron spectroscopy.[16−21] Although many examples of quantum beats among coherently excited states were reported, real-time probing of strongly coupled Fermi resonances in polyatomic molecular systems has been quite rare.

Photochemistry of phenol (C_6H_5OH) has been very intensively studied for recent decades not only because phenol itself is a very important biological building block but also because it is one of the prototypical systems undergoing the much-studied $\pi\sigma^*$-mediated relaxation dynamics on the excited-state.[22−29] Phenol in S_1 ($\pi\pi^*$) is strongly coupled to the upper-lying S_2 ($\pi\sigma^*$), which is repulsive along the O−H bond elongation coordinate. As a result, H atom tunneling takes place through the adiabatic reaction barrier under the S_1/S_2 conical intersection seam, and its height is predicted to be quite high assuring the prevalence of the tunneling process even at ~3500 cm^{-1} above the S_1 origin. Recent picosecond time-resolved spectroscopic studies have revealed that the H atom tunneling rate strongly depends on the low-frequency vibrational modes[30] seemingly orthogonal to the reaction coordinate, demonstrating that the tunneling dynamics is indeed multidimensional in nature.[31] The lifetime of S_1, which mainly reflects the tunneling rate, has been measured to be ~2 ns at the S_1 origin[32−37] and it decreases to ~0.8 ns at ~3600 cm^{-1} above S_1. Naturally, in these circumstances, it is an important question to what extent the energy randomization of intramolecular vibrational redistribution (IVR) plays a role during the concomitant tunneling process in terms of washing out the mode effect and thus averaging out the whole reaction dynamics governing reaction rates and energy disposals. In this work, we report the real-time observation of Fermi resonances and the energy flow dynamics among vibrational manifolds of the S_1 phenol undergoing the H atom tunneling predissociation.

A couple of well-separated peaks observed at S_1 internal energies (E_{int}) of 935 and 938 cm^{-1} in the S_1-S_0 nanosecond laser resonant two-photon ionization (R2PI) spectrum had been assigned as the 1^1 fundamental and $4^1 10b^1$ combination modes (Wilson notation), respectively.[38] Similarly, Bist et al. had reported the room-temperature gas-phase absorption spectrum showing closely spaced states in the same frequency region separated by ~3.37 cm^{-1}.[39] In the R2PI spectrum taken

Received: November 18, 2019
Accepted: December 12, 2019
Published: December 12, 2019

DOI: 10.1021/acs.jpclett.9b03393
J. Phys. Chem. Lett. 2020, 11, 161−165

here using the picosecond laser pulse with the temporal duration of 1.2 ps and the coherence width of ~25 cm^{-1}, these $1^1/4^1 10b^1$ bands with a separation of ~3 cm^{-1} are coherently excited, giving the necessary condition for the observation of quantum interferences thereafter. It should be noted here that the clear-cut characteristic of the Fermi-resonance is that the optically dark states get significant oscillatory strength via the coupling to the optically bright state. We have carried out Franck-Codon simulations for the S_1-S_0 transition of phenol (see the Supporting Information). It is evident that the Franck–Condon factor of the $4^1 10b^1$ combination band is predicted to be 4–6 orders of magnitude smaller than that of the 1^1 fundamental mode. However, in the experiment,[38] those coupled $4^1 10b^1$ and 1^1 modes show comparable intensities, strongly indicating that these modes belong to the Fermi doublet. Herein, including the $1^1/4^1 10b^1$ doublet, we have found several outstanding Fermi resonances in the S_1 phenol. Interferences from coherently excited eigenstates have been clearly observed in our picosecond time-resolved parent ion transients, giving the most precise energy gaps to date between strongly coupled eigenstates. Most surprisingly, it is found that the oscillatory amplitude of the quantum beat here is unusually large (*vide infra*) if the ionization energy is tuned just above the ionization threshold, strongly indicating that Fermi resonance eigenstates are almost completely decoupled into nonstationary zeroth-order quantum states in real time.

Prominent oscillatory features on the $[C_6H_5OH]^+$ transients are observed following the coherent population of $1^1/4^1 10b^1$ eigenstates of the S_1 phenol, giving the beating period of ~10 ps (Figure 1). The transient has been analyzed either by the Fourier-transform of the oscillating residuals obtained by subtracting the exponential decaying function from the experiment or by fitting the transient with a damping-cosine-implemented formula (see eq S1 in the Supporting Information), giving consistent values as listed in Table 1. The frequency gap ($\Delta\tilde{\nu}$) of the coherently excited $1^1/4^1 10b^1$ eigenstates is estimated to be 3.302 ± 0.001 cm^{-1}. This is the most precise value to date while it is widely in accord with the previously reported spectroscopic value of 3.37 or 3.3 cm^{-1}.[38,39] When the laser pulse populates another S_1 Fermi doublet located at 1564 and 1566 cm^{-1}, which had been assigned as 12^2 and $8a^1$ modes, respectively, the clear beating pattern has also been found, this time with the oscillation period of ~20 ps, Figure 2b. Transient analyses give the beating frequency of 1.655 ± 0.001 cm^{-1}. Notably, this is quite different from the previously reported literature value of 1.78 cm^{-1},[39] demonstrating that time-resolved measurement here gives the much-improved coupling constants in terms of both accuracy and precision, Table 1. Intriguingly, different types of $1^1/4^1 10b^1$ Fermi resonances are also found in combination with the $6a^1$ or 12^1 mode to give the $1^1 6a^1/4^1 10b^1 6a^1$ (1408/1412 cm^{-1}) or $1^1 12^1/4^1 10b^1 12^1$ Fermi doublet (1716/1719 cm^{-1}), respectively (see Figure S2 in the Supporting Information). The beating frequency analysis for the $1^1 6a^1/4^1 10b^1 6a^1$ and $1^1 12^1/4^1 10b^1 12^1$ doublet gives $\Delta\tilde{\nu}$ = 3.472 ± 0.004 or 3.201 ± 0.013 cm^{-1}, respectively.

The close proximity of two quantum levels belonging to the same irreducible symmetry species does not always guarantee the existence of a Fermi resonance. Moreover, it is not straightforward to observe quantum interferences experimentally as the total ionization cross section, for instance, would average out constructive and destructive quantum effects. In this regard, our clear-cut observation of quantum beat from the ion transients is quite notable. The oscillation amplitude is found to be strongly dependent on the probing wavelength (λ_{pr}) as its modulation depth exceeds more than 50% of the ion transients at the λ_{pr} = 309 nm for the $1^1/4^1 10b^1$ Fermi levels. The oscillation amplitude decreases sharply with the decrease of the probing wavelength, showing that it falls off less than 15% of the total ion signal at λ_{pr} = 301 nm (Figure 2). Considering the propensity rule of Δv = 0 in the D_0-S_1 transition, this indicates that the vibrational adiabatic ionization leads to the large fluctuations of the ionization cross section as the nearly degenerate zeroth-order S_1 states split remote in the D_0 state. For instance, theoretical calculations predict that the vibrational frequency of the $(4^1 10b^1)^+$ combination mode is much higher than that of the 1^{1+} mode in D_0 (see Table S1 in the Supporting Information). Therefore, the ionization cross section at λ_{pr} = 309 nm (32 362.5 cm^{-1}) should mostly represent the Franck–Condon (FC) overlap between 1^1 and 1^{1+} in S_1 and D_0, respectively. This acute FC overlap fades away in terms of its sensitivity on the probing spectral window as many more different vibrational modes of D_0 contribute to the total ionization cross-section as λ_{pr} is decreased to 301 nm (33 222.6 cm^{-1}), giving the significant reduction of the oscillation amplitude.

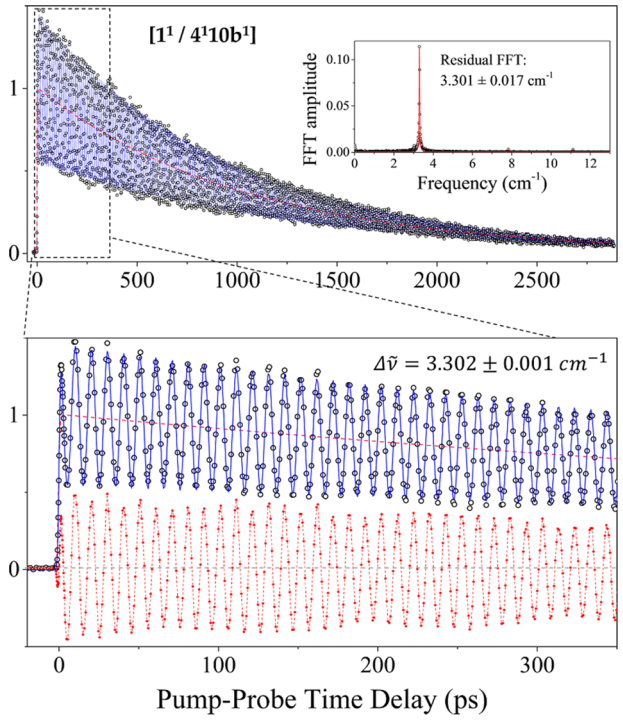

Figure 1. Picosecond pump–probe measurement of time-resolved $[C_6H_5OH]^+$ yield transient after the coherent excitation into $1^1/4^1 10b^1$ Fermi levels of S_1 phenol over the range of time delay up to ~2.9 ns. The probe wavelength for ionization (λ_{pr}) of 309 nm was irradiated after a certain time delay. Open circles are experimental data points, and the red filled symbols lying in the bottom are the residuals after subtraction of the exponentially decaying population kinetics (dashed red lines). The beating frequency, which corresponds to the energy separation between coherently populated Fermi levels, was analyzed by the formula described in eq S1 (the resultant fit given by blue solid) with the value of 3.302 cm^{-1}. Note that the observed oscillations are nondamping, but only decreases with the population kinetics. The Fourier-transform analysis (upper right inset) give a consistent frequency value of 3.301 cm^{-1}. See Figure S1 in the Supporting Information for an expanded view.

DOI: 10.1021/acs.jpclett.9b03393
J. Phys. Chem. Lett. 2020, 11, 161–165

Table 1. Beating Frequencies Derived from Picosecond Transients after Coherent Population of Fermi Levels, Compared with the Literature Values

band assignment[a]	S_1 energy (cm^{-1})[a]	$\Delta\tilde{\nu}$ ps beat (cm^{-1})[b]	τ_{dep} (ps)[c]	τ_{dIVR} (ps)[c]	$\Delta\tilde{\nu}$ (cm^{-1})[a]
$1^1/4^110b^1$	934.91/938.28	3.302 (3.301)	∞		3.37 (3.3)[d]
$1^16a^1/4^110b^16a^1$	1408.44/1411.93	3.472 (3.47)	1350		3.49
$12^2/8a^1$	1564.13/1565.91	1.655 (1.653)	440		1.78
$1^112^1/4^110b^112^1$	1716.46/1719.41	3.201 (3.16)	75	36	2.95

[a]Reference 39. The precision is stated to be about ±0.1 cm^{-1}. [b]Values in parentheses are obtained by Fourier-transforming the residuals after the subtraction of population kinetics. [c]See eq S1. [d]Reference 38.

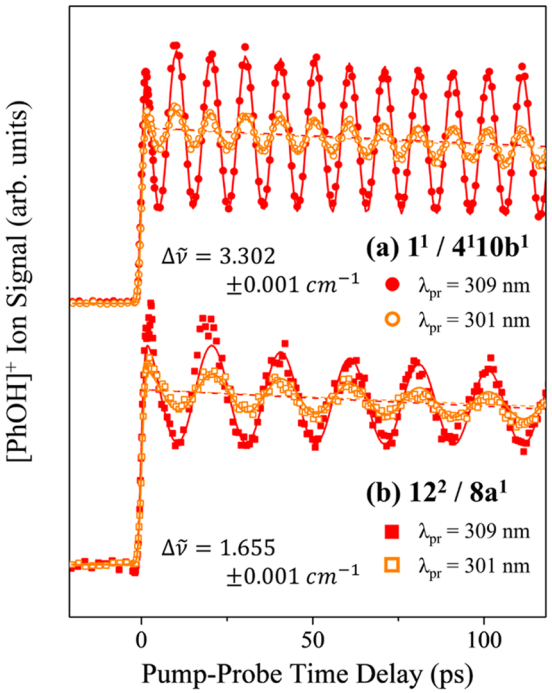

Figure 2. Early traces of picosecond-resolved $[C_6H_5OH]^+$ ion yield transients after the coherent excitation into (a) $1^1/4^110b^1$ and (b) $12^2/8a^1$ Fermi levels of S_1 phenol. Transients obtained with 301 and 309 nm ionization laser wavelengths are shown as open and filled symbols, respectively. Both analysis of Fourier transform of the residuals after the subtraction of the decay kinetics (dashed lines) and the cosine-implemented formula provide consistent result on the beating frequency of (a) 3.302 and (b) 1.655 cm^{-1}. For transients over the extended range of time delay, see Figure S1 in the Supporting Information.

Further variation of λ_{pr} into the shorter wavelength results in the entire absence of the oscillating feature (see Figures S2 and S3 in the Supporting Information). This phenomenon could also be seen for $12^2/8a^1$ and all other Fermi levels, giving the interference pattern where the oscillating depth is largely dependent on λ_{pr}.

Decoupling of Fermi resonances into the zeroth-order quantum states in real time could be rationalized by the following simple model. Namely, we could represent Fermi resonant eigenstates as follows:

$$|i\rangle = \frac{1}{\sqrt{2}}(|\phi_1\rangle + |\phi_2\rangle) \qquad |j\rangle = \frac{1}{\sqrt{2}}(|\phi_1\rangle - |\phi_2\rangle)$$

Here $|i\rangle$ and $|j\rangle$ are molecular eigenstates whereas $|\phi_1\rangle$ and $|\phi_2\rangle$ are zeroth-order states where magnitudes of coupling coefficients are assumed to be equivalent. The coherently excited state by the picosecond laser pulse is then the superposition of $|i\rangle$ and $|j\rangle$, giving the time-dependent wave function, $\Psi(t)$.

$$\Psi(t) = \frac{1}{\sqrt{2}}(|i\rangle e^{-i(E_i/\hbar)t} + |j\rangle e^{-i(E_i/\hbar)t}) = \frac{1}{2}|\phi_1\rangle\{e^{-i(E_i/\hbar)t} + e^{-i(E_i/\hbar)t}\} + \frac{1}{2}|\phi_2\rangle \{e^{-i(E_i/\hbar)t} - e^{-i(E_i/\hbar)t}\}$$

The ionization cross-section near the ionization threshold will reflect the projection of $\Psi(t)$ onto $|\phi_1^+\rangle$, representing the quantum-mechanical contribution of $|\phi_1\rangle$ in $\Psi(t)$ as the low-lying $|\phi_1^+\rangle$ and high-lying $|\phi_2^+\rangle$ are decoupled and well separated in the D_0 state (*vide supra*).

$$\langle\phi_1^+|\Psi(t)\rangle \cong \frac{1}{2}\langle\phi_1^+|\phi_1\rangle\{e^{-i(E_i/\hbar)t} + e^{-i(E_i/\hbar)t}\}$$

Here, according to the propensity rule of $\Delta v = 0$ in the ionization, $\langle\phi_1^+|\phi_2\rangle \cong 0$ should be a good approximation. The ionization cross-section near the threshold then will be proportional to $|\langle\phi_1^+|\Psi(t)\rangle|^2$ as follows where $\langle\phi_1^+|\phi_1\rangle \equiv c_1$.

$$|\langle\phi_1^+|\Psi(t)\rangle|^2 = \frac{1}{2}c_1\{e^{-i(E_i/\hbar)t} + e^{-i(E_i/\hbar)t}\} \times \frac{1}{2}c_1^*\{e^{i(E_i/\hbar)t} + e^{i(E_i/\hbar)t}\} = \frac{1}{2}c_1^2\left[1 + \cos\left(\frac{E_i - E_j}{\hbar}t\right)\right]$$

This value spans from zero to c_1^2 as a function of time, demonstrating that the coherently excited Fermi doublet could be completely decoupled into the zero-order state according to the oscillatory quantum beat in real time.

In fact, coherently populating Fermi resonance levels could be regarded as one of the prototypical examples of the restricted IVR as it represents the typical energy flow between the optically bright zeroth-order state and a nearly isoenergetic yet optically dark quantum state if the terminology of IVR is used in the strict way. As long as further IVR into dark quantum manifolds is not activated, interferences due to coherent excitation of Fermi eigenstates are expected to persist during the whole S_1 lifetime. However, if the "so-called" dissipative IVR takes in action, then such an interference would dephase accordingly. Namely, whereas the S_1 lifetime of phenol is largely determined by the H atom tunneling rate, the oscillation amplitude could decrease with time as the interference of Fermi levels dephases as IVR into dark manifolds intrudes the otherwise two-state coupling of Fermi resonance. From the fits to the experiment using eq S1, the dephasing time constants (τ_{dep}) of infinity or ~400 ps are obtained for the $1^1/4^110b^1$ (Figure 1) and $12^2/8a^1$ Fermi levels, respectively (Figure S1). This is quite reasonable as the

DOI: 10.1021/acs.jpclett.9b03393
J. Phys. Chem. Lett. 2020, 11, 161−165

S_1 internal energy of $1^1/4^1 10b^1$ is centered at ~937 cm^{-1} while that of $12^2/8a^1$ is located at ~1565 cm^{-1}. As such, the dissipative IVR is not activated yet within the S_1 lifetime of ~1.0 ns at ~937 cm^{-1}. Meanwhile, the dissipative IVR beyond Fermi-type coupling occurs at E_{int} ~ 1565 cm^{-1} with a rate faster than tunneling. In retrospect, this behavior seems to be quite consistent with recently measured tunneling rate constants of the S_1 phenol which show large fluctuations at E_{int} lower than ~1300 cm^{-1} and become monotonic at the higher internal energy. It is notable that the dephasing rate gets increased sharply with increasing the internal energy, giving τ_{dep} of ~75 ps at E_{int} ~ 1718 cm^{-1} associated with the $1^1 12^1/4^1 10b^1 12^1$ Fermi doublet (Figure S2b). In addition, the fast decaying component with the ultrashort lifetime less than tens of picoseconds has been found in the initial part of the $1^1 12^1/4^1 10b^1 12^1$ transient. This ultrafast decaying component of the transient should be associated with IVR in S_1 as the ionization cross-section becomes rapidly dispersive with the accompanying mode-randomization.

It is notable again that the Fermi-type interference survives during the entire S_1 lifetime of phenol even at the internal energy of ~937 cm^{-1}, giving the full support for the observation of the strong mode-dependent tunneling rates. This also promises the mode-selective chemistry of the excited polyatomic systems as the mode randomization is found to be rather slow compared with the reaction rate. Although low-frequency modes are hardly associated with the reaction coordinate of the specific bond cleavage, for instance, their excitations are closely related to the subtle structural changes that are quite often very critical in nonadiabatic transitions on the multidimensional conical intersection seam or in shaping the adiabatic transition states diversely defined along the orthogonal conformational coordinates. In this regard, exploration of mode-effect on excited-state dynamics and its relation to the energy flow among close-lying quantum states as observed here will shed new light on the structure−function relationship in a number of molecular systems.

EXPERIMENTAL METHODS

Experimental methods of frequency- and time-resolved pump−probe ion yield spectroscopy have been recently given elsewhere.[31] Briefly, tunable laser pulses in the ultraviolet wavelength range are generated from two optical parametric amplifiers (TOPAS-800 ps, light conversion) pumped by the 50:50 split fundamental outputs from the 1 kHz picosecond Ti:sapphire regenerative amplifier system (Legend Elite-P, coherent). Pump and probe pulses interact with the gas mixture in the supersonic jet operated by a 200 Hz pulsed Even-Lavie valve. The polarization angle between pump and probe was set to 54.7° (magic angle) to rule out any rotational alignment effect. The temporal delay between pump and probe pulses (Δt) were scanned using a broadband hollow retroreflector (UBBR2.5-1UV, Newport) mounted on a computer-controlled 220 mm optical delay line stage (DDS220, Thorlabs), where the delay step sizes of 0.8 ps are used for the range of monitoring oscillatory features.

ASSOCIATED CONTENT

Supporting Information

The Supporting Information is available free of charge at https://pubs.acs.org/doi/10.1021/acs.jpclett.9b03393.

Details in fitting procedure of the transients with oscillations; transients in the full range of time delay along with the beating frequency analyses; transients for the additional Fermi levels of combined $1^1/4^1 10b^1$ with the modes 6a and 12; comparison of transients for S_1 vibronic levels near $1^1/4^1 10b^1$ with various probe wavelengths; results of the harmonic frequency calculations; additional notes on the $S_0 \rightarrow S_1$ Franck−Condon simulation; time-dependent Fermi doublet in the experiment (PDF)

AUTHOR INFORMATION

Corresponding Author

*E-mail: sangkyukim@kaist.ac.kr.

ORCID

Kyung Chul Woo: 0000-0002-9387-9397

Sang Kyu Kim: 0000-0003-4803-1327

Present Address

†Division of Chemistry and Biological Chemistry, School of Physical and Mathematical Sciences, Nanyang Technological University, Singapore 637371.

Notes

The authors declare no competing financial interest.

ACKNOWLEDGMENTS

This work was financially supported by the National Research Foundation under the Project Number 2018R1A2B3004534.

REFERENCES

(1) Blau, H. H.; Nielsen, H. H. The infrared absorption spectrum of formaldehyde vapor. *J. Mol. Spectrosc.* **1957**, *1* (1), 124−132.

(2) Morino, Y.; Nakamura, J.; Yamamoto, S. Fermi resonances in the rotational structure of the infrared spectra of methyl iodide. *J. Mol. Spectrosc.* **1967**, *22* (1), 34−48.

(3) Lucazeau, G.; Sandorfy, C. The near-infrared spectra of some simple aldehydes. *Can. J. Chem.* **1970**, *48* (23), 3694−3703.

(4) Stidham, H. D.; Dilella, D. P. Vibrational perturbation: A chemical aid to assignment. I-Fermi resonance in the ν_8 region of isotopic pyridines. *J. Raman Spectrosc.* **1979**, *8* (3), 180−184.

(5) Wilson, H. W.; Macnamee, R. W.; Durig, J. R. Raman spectra of gases: 24-Phenol. *J. Raman Spectrosc.* **1981**, *11* (4), 252−255.

(6) Abbate, S.; Wunder, S. L.; Zerbi, G. Conformational dependence of Fermi resonances in n-alkanes. Raman spectrum of 1,1,1,4,4,4-hexadeuteriobutane. *J. Phys. Chem.* **1984**, *88* (3), 593−600.

(7) Sokołowska, A.; Kęcki, Z. Inter- and intra-molecular coupling and Fermi resonance in the Raman spectra of liquid water. *J. Raman Spectrosc.* **1986**, *17* (1), 29−33.

(8) Knight, A. E. W.; Kable, S. H. The $S_1-S_0(^1B_{2u}-^1A_g)$ transition of *p*-difluorobenzene cooled in a supersonic free jet expansion. Excitation and dispersed fluorescence spectra, vibrational assignments, Fermi resonances, and forbidden transitions. *J. Chem. Phys.* **1988**, *89* (12), 7139−7160.

(9) Troxler, T. S_1-S_0 Electronic Spectroscopy and ab Initio Calculations of *cis*-2-Methoxynaphthalene. *J. Phys. Chem. A* **1998**, *102* (25), 4775−4787.

(10) Isozaki, T.; Sakeda, K.; Suzuki, T.; Ichimura, T. Fluorescence spectroscopy of jet-cooled o-fluoroanisole: Mixing through Duschinsky effect and Fermi resonance. *J. Chem. Phys.* **2010**, *132* (21), 214308.

(11) Brand, C.; Küpper, J.; Pratt, D. W.; Leo Meerts, W.; Krügler, D.; Tatchen, J.; Schmitt, M. Vibronic coupling in indole: I. Theoretical description of the $^1L_a-^1L_b$ interaction and the electronic spectrum. *Phys. Chem. Chem. Phys.* **2010**, *12* (19), 4968−4979.

(12) Gmerek, F.; Stuhlmann, B.; Álvarez-Valtierra, L.; Pratt, D. W.; Schmitt, M. Electronic spectra of 2- and 3-tolunitrile in the gas phase.

DOI: 10.1021/acs.jpclett.9b03393
J. Phys. Chem. Lett. 2020, 11, 161−165

II. Geometry changes from Franck-Condon fits of fluorescence emission spectra. *J. Chem. Phys.* **2016**, *144* (8), 084304.
(13) Lambert, W. R.; Felker, P. M.; Zewail, A. H. Picosecond excitation and selective intramolecular rates in supersonic molecular beams. II. Intramolecular quantum beats and IVR. *J. Chem. Phys.* **1984**, *81* (5), 2217−2232.
(14) Felker, P. M.; Zewail, A. H. Dynamics of intramolecular vibrational-energy redistribution (IVR). II. Excess energy dependence. *J. Chem. Phys.* **1985**, *82* (7), 2975−2993.
(15) Li, S.; Long, J.; Ling, F.; Wang, Y.; Song, X.; Zhang, S.; Zhang, B. Real-time visualization of the vibrational wavepacket dynamics in electronically excited pyrimidine via femtosecond time-resolved photoelectron imaging. *J. Chem. Phys.* **2017**, *147* (4), 044309.
(16) Hammond, C. J.; Reid, K. L.; Ronayne, K. L. Observation of a simple vibrational wavepacket in a polyatomic molecule via time-resolved photoelectron velocity-map imaging: A prototype for time-resolved IVR studies. *J. Chem. Phys.* **2006**, *124* (20), 201102.
(17) Davies, J. A.; Green, A. M.; Reid, K. L. Deducing anharmonic coupling matrix elements from picosecond time-resolved photoelectron spectra: application to S_1 toluene at low vibrational energy. *Phys. Chem. Chem. Phys.* **2010**, *12* (33), 9872−9883.
(18) Long, J.; Qin, C.; Liu, Y.; Zhang, S.; Zhang, B. Direct imaging of the Fermi resonance interaction in para-difluorobenzene: A special insight into energy redistributions in the S_1 low-energy regime. *Phys. Rev. A: At., Mol., Opt. Phys.* **2011**, *84* (6), 063409.
(19) Davies, J. A.; Reid, K. L. Elucidating Quantum Number-Dependent Coupling Matrix Elements Using Picosecond Time-Resolved Photoelectron Spectroscopy. *Phys. Rev. Lett.* **2012**, *109* (19), 193004.
(20) Gardner, A. M.; Green, A. M.; Tamé-Reyes, V. M.; Reid, K. L.; Davies, J. A.; Parkes, V. H. K.; Wright, T. G. The 700−1500 cm^{-1} region of the S_1 ($\tilde{A}^1B_2$) state of toluene studied with resonance-enhanced multiphoton ionization (REMPI), zero-kinetic-energy (ZEKE) spectroscopy, and time-resolved slow-electron velocity-map imaging (tr-SEVI) spectroscopy. *J. Chem. Phys.* **2014**, *140* (11), 114308.
(21) Kemp, D. J.; Gardner, A. M.; Tuttle, W. D.; Midgley, J.; Reid, K. L.; Wright, T. G. Identifying complex Fermi resonances in p-difluorobenzene using zero-electron-kinetic-energy (ZEKE) spectroscopy. *J. Chem. Phys.* **2018**, *149* (9), 094301.
(22) Sobolewski, A. L.; Domcke, W.; Dedonder-Lardeux, C.; Jouvet, C. Excited-state hydrogen detachment and hydrogen transfer driven by repulsive $^1\pi\sigma^*$ states: A new paradigm for nonradiative decay in aromatic biomolecules. *Phys. Chem. Chem. Phys.* **2002**, *4* (7), 1093−1100.
(23) Tseng, C. M.; Lee, Y. T.; Ni, C. K. H atom elimination from the $\pi\sigma^*$ state in the photodissociation of phenol. *J. Chem. Phys.* **2004**, *121* (6), 2459−61.
(24) Lan, Z.; Domcke, W.; Vallet, V.; Sobolewski, A. L.; Mahapatra, S. Time-dependent quantum wave-packet description of the $^1\pi\sigma^*$ photochemistry of phenol. *J. Chem. Phys.* **2005**, *122* (22), 224315.
(25) Nix, M. G. D.; Devine, A. L.; Cronin, B.; Dixon, R. N.; Ashfold, M. N. R. High resolution photofragment translational spectroscopy studies of the near ultraviolet photolysis of phenol. *J. Chem. Phys.* **2006**, *125* (13), 133318.
(26) Dixon, R. N.; Oliver, T. A. A.; Ashfold, M. N. R. Tunnelling under a conical intersection: Application to the product vibrational state distributions in the UV photodissociation of phenols. *J. Chem. Phys.* **2011**, *134* (19), 194303.
(27) Roberts, G. M.; Chatterley, A. S.; Young, J. D.; Stavros, V. G. Direct Observation of Hydrogen Tunneling Dynamics in Photoexcited Phenol. *J. Phys. Chem. Lett.* **2012**, *3* (3), 348−352.
(28) Xu, X.; Zheng, J.; Yang, K. R.; Truhlar, D. G. Photodissociation dynamics of phenol: multistate trajectory simulations including tunneling. *J. Am. Chem. Soc.* **2014**, *136* (46), 16378−86.
(29) Xie, C.; Ma, J.; Zhu, X.; Yarkony, D. R.; Xie, D.; Guo, H. Nonadiabatic Tunneling in Photodissociation of Phenol. *J. Am. Chem. Soc.* **2016**, *138* (25), 7828−7831.
(30) Lai, H. Y.; Jhang, W. R.; Tseng, C.-M. Communication: Mode-dependent excited-state lifetime of phenol under the S_1/S_2 conical intersection. *J. Chem. Phys.* **2018**, *149* (3), 031104.
(31) Woo, K. C.; Kim, S. K. Multidimensional H Atom Tunneling Dynamics of Phenol: Interplay between Vibrations and Tunneling. *J. Phys. Chem. A* **2019**, *123* (8), 1529−1537.
(32) Sur, A.; Johnson, P. M. Radiationless transitions in gas phase phenol and the effects of hydrogen bonding. *J. Chem. Phys.* **1986**, *84* (3), 1206−1209.
(33) Lipert, R. J.; Bermudez, G.; Colson, S. D. Pathways of S_1 decay in phenol, indoles, and water complexes of phenol and indole in a free jet expansion. *J. Phys. Chem.* **1988**, *92* (13), 3801−3805.
(34) Berden, G.; Meerts, W. L.; Schmitt, M.; Kleinermanns, K. High resolution UV spectroscopy of phenol and the hydrogen bonded phenol-water cluster. *J. Chem. Phys.* **1996**, *104* (3), 972−982.
(35) Grégoire, G.; Dedonder-Lardeux, C.; Jouvet, C.; Martrenchard, S.; Solgadi, D. Has the Excited State Proton Transfer Ever Been Observed in Phenol−$(NH_3)_n$ Molecular Clusters? *J. Phys. Chem. A* **2001**, *105* (25), 5971−5976.
(36) Ratzer, C.; Küpper, J.; Spangenberg, D.; Schmitt, M. The structure of phenol in the S_1-state determined by high resolution UV-spectroscopy. *Chem. Phys.* **2002**, *283* (1−2), 153−169.
(37) Pino, G. A.; Oldani, A. N.; Marceca, E.; Fujii, M.; Ishiuchi, S.-I.; Miyazaki, M.; Broquier, M.; Dedonder, C.; Jouvet, C. Excited state hydrogen transfer dynamics in substituted phenols and their complexes with ammonia: $\pi\pi^*$-$\pi\sigma^*$ energy gap propensity and *ortho*-substitution effect. *J. Chem. Phys.* **2010**, *133* (12), 124313.
(38) Dopfer, O. *Ph.D. Dissertation*. Technische Universitat Munchen, 1994.
(39) Bist, H. D.; Brand, J. C. D.; Williams, D. R. The 2750-Å electronic band system of phenol: Part I. The in-plane vibrational spectrum. *J. Mol. Spectrosc.* **1966**, *21* (1), 76−98.

DOI: 10.1021/acs.jpclett.9b03393
J. Phys. Chem. Lett. 2020, 11, 161−165